FRONTAL HEAD-ON CAR-TO-HEAVY GOODS VEHICLE CRASHES EFFECT ON THE RESTRAINT SYSTEM

Martin Östling
Autoliv Research
Sweden

Linda Eriksson, Mikael Dahlgren
Autoliv
Sweden

Jason Forman
University of Virginia Center for Applied Biomechanics
U.S.A.

Paper Number 23-0198

ABSTRACT

For car occupants in Europe, a car-to-HGV (heavy goods vehicle) crash is the third most frequent fatal crash type after single and car-to-car crashes. Within car-to-HGV fatal crashes, frontal head-on crashes are most common. These crashes can result in larger structural deformation of the car or higher velocity changes and accelerations than single or car-to-car crashes typically do.

Structural compatibility and energy absorbing structures are prerequisites for good crashworthiness, so also for severe head on car-to-HGV crashes. If the car compartment can be kept intact there is a potential to improve the current state-of-the-art frontal restraint systems to provide the occupant with good protection also in high-severity car-to-HGV crashes.

The goal of this study was to identify potential limitations in a state-of-the-art frontal restraint system in high-severity car-to-HGV head-on crashes with an intact compartment and propose improvements to the restraint system to reduce and balance the risk of injury for all body regions.

Finite element simulations were performed using a frontal sled interior model with a geometry representing a mid-size sedan. The frontal sled model was equipped with the semi-rigid seat, a generic seat consisting of spring-loaded seat and submarining pans, developed to represent the characteristics of a front seat, and a seat integrated belt system consisting of a shoulder belt retractor with a 4 kN load limiter and a 2 kN pretensioner, and a 2 kN lap belt pretensioner. Further, the model was equipped with a driver airbag, a steering wheel, a collapsible steering column, a knee bolster, and a foot support. The model was validated by means of mechanical sled tests using generic 40 and 56 km/h full frontal rigid barrier crash pulses and THOR-50M v1.9. After validation the performance of the restraint system was evaluated with the THOR-50M by implementing crash pulses from two car-to-HGV head-on crashes.

For both car-to-HGV crash pulses there were severe strikethroughs of the restraint system. Improved seat stiffness, increased shoulder belt load limiter force, and increased knee bolster energy absorption prevented the strikethroughs and reduced the injury criteria values. However, the injury criteria values were still higher than current NCAP performance limits for most of the body regions. To guide the development of adaptive occupant protection tailored for high severity crashes, injury criteria targets are required. Such targets should be balanced between feasibility and still challenging enough to prompt improvements relative to the current state of risks.

Occupant protection in different crash severities is of high priority. The occupant protection system should be designed to be adaptive to the crash, i.e. more compliant in low-severity crashes and stiffer in high-severity crashes. Current occupant restraint systems are most likely capable of the proposed improvements with existing technologies. However, they are currently not designed with the level of adaptivity that this study indicates may be beneficial. More research is needed to develop injury criteria target values for survival in high severity crashes, as well as sensors that distinguish between low-, mid- and high-severity crashes with the purpose to adapt the restraint system thereafter.

INTRODUCTION

In 2019, about 22,700 road traffic related fatalities occurred in the European Union (EU) and more than 1.2 million people were injured [1]. Car occupants represent approximately 44% (10,090) of the fatalities in the EU [2]. Car drivers represent 71% of fatally injured car occupants, where of 82% were males and 18% were females [2]. Moreover, car occupant fatalities in car-to-HGV crashes have a larger proportion of occupants in the age group of 25 to 64 year-olds (65%) [3] compared to all car fatalities (58%) [4].

Although heavy good vehicles (HGVs) were only involved in 4.5% of all crashes, HGVs were involved in approximately 14% of all road fatalities in the EU in 2019 [3-4]. A car-to-HGV crash was the third most frequent fatal crash mode for car occupants in the EU (1557 fatalities), after single car crashes (4400 fatalities), and car-to-car crashes (3067 fatalities) [5]. The consequence of a car-to-HGV crash is often serious for the car occupants due to the incompatibility in mass and vehicle structure stiffness and geometry [6-11]. Most of the fatal crashes involving HGVs occurred on rural roads (53%), followed by highways (24%) and urban roads 23% [4]. The largest proportion of these crashes occurred on road stretches (82%) and only few occurred at intersections (9%) or other places [4]. The most frequent fatal car-to-HGV crash in the EU is a head-on crash on a rural road stretch [12-13].

Car crash pulses are a prerequisite when investigating the risk of injury for car occupants using finite element (FE) simulations. The German In-Depth Accident Study (GIDAS) data was analysed to describe car-to-HGV head-on crashes at a level of detail that enable setting up vehicle-to-vehicle FE simulation to generate crash pulses for the car [13]. Car-to-HGV crash configuration distributions were statistically described using relevant kinematic parameters from GIDAS (collision velocities of car and HGV, relative velocities, impact angles, hit points, vehicle weights). Using this data set as starting point, car crash pulses from car-to-HGV head on crashes were created by FE simulations of a 1.7-ton car and a 7.9-ton HGV including a frontal underride protection device (FUPD) [14]. 12 different crash configurations were simulated by varying the impact velocities of the two vehicles (car velocity 39 km/h and HGV velocity 36 km/h, and car velocity 56 km/h and HGV velocity 53 km/h), the impact overlaps (50% and 80%) and the impact angle (0°, 30° and -30°). Peak acceleration and delta velocity from the left sill, the compartment structural integrity, and pulse duration were analysed to identify relevant car crash pulses to be used for car occupant protection simulations. Structural integrity was evaluated because it remains a prerequisite for the occupant restraint system to be effective; if there is major A-pillar collapse the occupant protection system will be of less importance for the crash outcome. Two crash configurations out of the 12 were recommended for car occupant protection simulations:

1. 56/53 (Car/HGV) km/h, 50% overlap in 30° angle. This crash configuration was selected because it had a relatively long duration when compared to a standard 56 km/h full front rigid barrier test. Such crash pulse characteristics are challenging for a state-of the-art restraint system in terms of for example the stand-up time for the driver airbag. This crash pulse is referred to as the *long duration crash pulse*. This pulse has a peak acceleration of 66g and a delta velocity of 105 km/h.

2. 56/53 (Car/HGV) km/h, 80% overlap in 0° angle. This crash configuration was selected because it had a relatively high acceleration level when compared to a standard 56 km/h full front rigid barrier test. Such crash pulse characteristics are challenging for a state-of the-art restraint system in terms of for example strikethrough of the driver airbag because the high acceleration will lead to a higher change in velocity to the interior. This crash pulse is referred to as the *high acceleration crash pulse*. This pulse has a peak acceleration of 91g and a delta velocity of 97 km/h.

Occupant protection in high-severity collisions is not a new concept. In an investigation of 80 km/h full frontal rigid barrier (FFRB) crashes, it was concluded that “with proper design of an adaptive restraint system efficient occupant protection can be achieved at both high and very high impact velocities” [15].

The aim of this study was to identify potential occupant protection limitations in a state-of-the-art frontal restraint system in high-severity car-to-HGV head-on crashes with an intact compartment, defined by [14], and propose potential improvements to the restraint system to reduce and balance the risk of injury to equal level for all body regions [16].

METHODS

The methodology chapter is divided into four sub-sections describing the different steps in the investigation. First, we describe the frontal sled FE model incorporating a state-of-the-art frontal driver restraint system. Second, we describe the validation of the frontal sled model by means of mechanical sled tests using generic crash pulses representing full frontal rigid barrier (FFRB) tests in 40 km/h and 56 km/h. Third, we describe the implementation of two car-to-HGV head-on crash pulses from [14] and its effect to the system model and identify limitations in the state-of-the-art frontal restraint system in terms of occupant protection. Fourth, we describe potential improvements of the state-of-the-art frontal driver restraint system with the aim to reduce the risk of injury in car-to-HGV head-on crashes referencing target injury criteria values for high severity crashes identified in a parallel investigation [16].

Description of the frontal sled FE model

A frontal sled FE model including a state-of-the-art driver restraint system was developed using LS-Dyna, R9.3.1 r140922, LSTC. The frontal sled model includes: generic floor geometry and foot support; semi-rigid seat [17]; seat-back to support the occupant; generic knee bolster (Ethafoam 220 mounted to a rigid plate); seat integrated belt geometry (belt-in-seat) with a ridgid attached belt guide in the seatback, a shoulder belt retractor with a 2 kN pretensioner and a 4 kN load limiter, a wire buckle, a crash-locking tongue, and a 2 kN lap belt pretensioner; generic stroking steering column at a force limit of 5.5 kN and a stroke of 85 mm; and a steering wheel with a generic driver airbag module including a cushion with coated fabric, vent holes and an inflator.

The driver was represented by the THOR-50M (Test device for Human Occupant Restraint 50th percentile adult male dummy) based on the occupant characteristics in terms of sex and age observed in the field data investigations of fatal car-to-HGV crashes [2-4]. The THOR-50M v1.9 Euro NCAP version from Humanetics Inc was positioned with the H-point 4 mm behind and 29 mm up from the seat reference points (*Figure 1*).

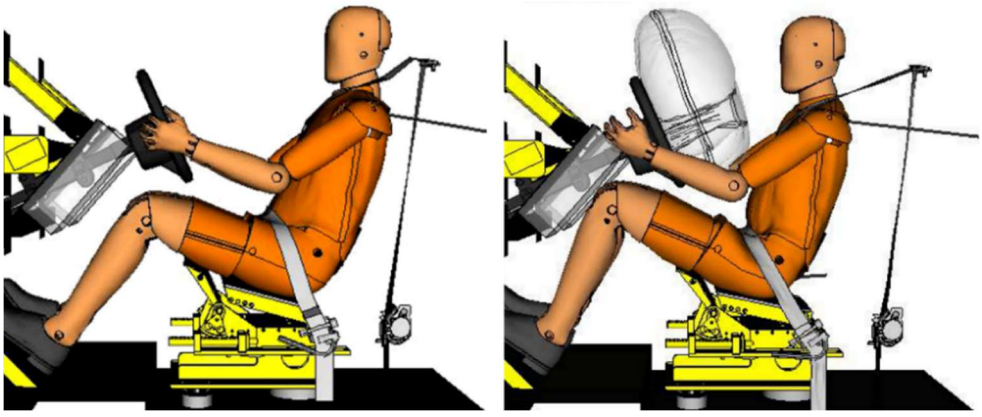

Figure 1. **THOR-50M in the frontal sled FE model with a seat integrated belt system at two different time steps. Left: Figure plotted at 0 ms. Right: Figure plotted at 40 ms with the generic 56 km/h FFRB crash pulse applied.** ***Note: for visibility reason the seat back is removed in these to figures.***

Validation of the frontal sled FE model

The frontal sled model was validated by means of mechanical sled tests, see *Figure 2*. For the validation, repeated tests were conducted using two different generic crash pulses representing a 40 km/h and a 56 km/h FFRB crash [18], in total four sled tests. The model correlated well with the tests; validation results are described in the appendix.

Simulation of 56 km/h FFRB and car-to-HGV head-on crash pulses

The two car-to-HGV crash pulses recommended in [14] were implemented in the validated frontal sled model, *Figure 3*. To simplify the simulation only the x-component of the car crash pulses from [14] were used. Simulations with the state-of-the-art restraint system with the THOR-50M as driver were then conducted. The THOR-50M response in the two high-severity car-to-HGV crash pulses were compared to the generic 56 km/h FFRB crash pulse and used to identify potential limitations in the state-of-the-art restraint system.

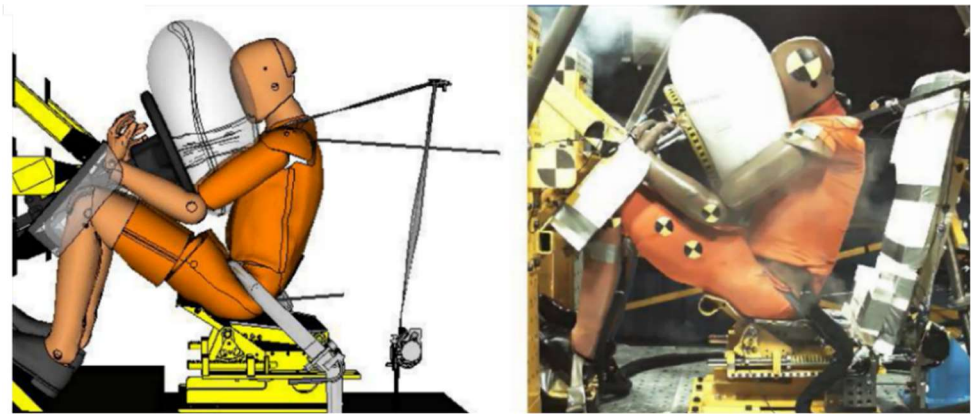

Figure 2. **Virtual and physical version of the frontal sled with the seat integrated belt in the 56 km/h FFRB crash pulse. Left: Frontal sled FE model plotted at 60 ms. Right: Sled test plotted at 60 ms.**

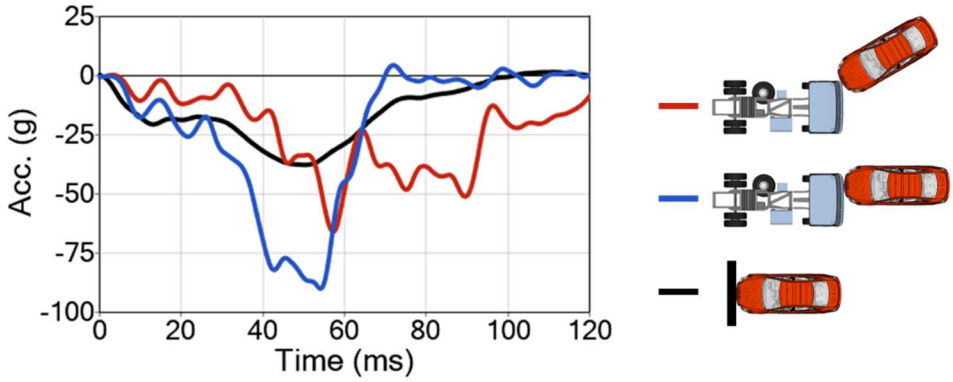

Figure 3. **Crash pulses used in the simulation study. Generic 56 km/h FFRB crash pulse in black [18]. High acceleration crash pulse, peak acceleration of 91g and a delta velocity of 97 km/h in blue [14]. Long duration crash pulse, peak acceleration of 66g and a delta velocity of 105 km/h in red [14].**

Target criteria and improvements of state-of-the-art restraint system

Target criteria addressing both occupant kinematics and risk of injury were identified. For occupant kinematics three criteria were identified:

1. No head-to-steering wheel strikethrough, i.e., avoid hard contact between the head and the steering wheel.
2. No knee-to-knee bolster strikethrough, i.e., avoid hard contact between knee and underlaying structure.
3. No pelvis-to-seat pan strikethrough, i.e., avoid hard contact between pelvis and underlaying structure.

Target injury criteria values for THOR-50M associated with a 40% risk of injury for all body regions [19] were identified and proposed in a parallel investigation [16] and are presented in *Table 1*.

Guided by these target criteria, improvements were made to the state-of-the-art restraint system with the purpose to improve the occupant protection of THOR-50M when exposed for the car-to-HGV crash pulses. The target with the improvements was to keep the design of the state-of-the-art restraint system, e.g., not adding any unconventional restraint components such as an extra belt [20], but to add a second functionality level to balance the higher energy from the car-to-HGV crash pulse. Adding such functionality to the occupant restraint system based on the crash severity level makes the occupant restraint system adaptable. This can be exemplified by implementing a higher load limiting force in the shoulder belt. However, improvements might be best fulfilled by adding an already state-of-the-art component, e.g., a knee airbag and/or a seat pan mounted airbag, also called pelvis restraint cushion [21-22].

Table 1.
THOR-50M target injury criteria values proposed for high severity car crashes, balanced for equal risk of injury for all body regions [16].

Criteria	Unit	Risk	Value
HIC15 (AIS3+)		40%	1430
BrIC (AIS3+)		40%	0.89
Nij (AIS3+)	mm	40%	1.04
Chest deflection (3+ fracture 40 years)	mm	40%	46.5
Chest deflection (6+ fracture 40 years)	mm	40%	56.5
Acetabulum resultant force (AIS2+), 15° Femur flexion	N	40%	3180
Acetabulum resultant force (AIS2+), 0° Femur flexion	N	40%	3910
Femur compression force (AIS2+)	N	40%	9800
Upper Tibia axial force (AIS2+)	kN	40%	6.5
Lower Tibia axial force (AIS2+)	kN	40%	7.15
Tibia bending moment (AIS2+)	Nm	40%	290
Revised Tibia index (AIS2+)		40%	1.13

Several simulation iterations were performed to identify how the state-of-the-art restraint system could be improved to fulfil the set targets. Avoiding strikethrough of the head, knees and pelvis were considered as the top initial priorities for tuning the restraint system, and the resulting THOR-50M injury criteria values from that initial tuning were then compared to the values of *Table 1* to identify potential areas for further refinement.

RESULTS

Simulation results from 56 km/h FFRB crash pulse with the state-of-the-art restraint system

The state-of-the-art restraint system performed well in the generic 56 km/h FFRB crash pulse, seen in a controlled kinematic of the THOR-50M, e.g. >50 mm remaining distance between the head and the steering wheel, and predicted overall low risk of injury, except for the chest and the acetabulum *Table 2*. However, if the risk function for 0-degree femur flexion [19] is applied as proposed by [16] the risk of acetabulum fracture is reduced from 71% to 37%. Corresponding seatbelt characteristic, driver airbag pressure, and steering column force and stroke are presented in *Figure 4* and *Figure 5*. The driver airbag pressure reached almost 50 kPa, the lap belt forces reached approximately 8 kN and the steering column reached its end position at approximately 90 ms with a force of approximately 8 kN.

Simulation results from car-to-HGV crash pulses with the state-of-the-art restraint system

Both car-to-HGV head-on crash pulses were challenging for the-state-of-the-art restraint system, reaching its limit in terms of controlled kinematics (head-to-steering wheel strikethrough). The *high acceleration crash pulse* was the worst crash pulse among the two car-to-HGV crash pulses as it resulted in an earlier strikethrough of the driver airbag (head-to-steering wheel strikethrough), high pelvis acceleration (pelvis-to-seat pan strikethrough), and high femur compression forces (knee-to-knee bolster strikethrough), see *Figure 6* and *Figure 7*.

A visualisation of the initial THOR-50M position, at maximum pelvis forward displacement (knee-to-knee bolster strikethrough and pelvis-to-seat pan strikethrough), and at maximum chest forward displacement (head-to-steering wheel contact) for the simulation with the *high acceleration crash pulse* is presented in *Figure 8*.

Again, corresponding seatbelt characteristics, driver airbag pressure, and steering column force and stroke for the state-of-the-art restraint system are presented in *Figure 4* and *Figure 5*. For the *high acceleration crash pulse,* the driver airbag pressure reached above 80 kPa, the lap belt forces reached above 12 kN and the steering column reached its end position at approximately 70 ms at a force of above 20 kN.

In terms of injury criteria values the *high acceleration crash pulse* was the more challenging crash pulse, seen in risk of injury between 38% and 100% compared to 1% to 94% for the long duration crash pulse, *Table 2*. Therefore, the improvements of the state-of-the art restraint system were explored with focus on the *high acceleration crash pulse* and then checked with the *long duration crash pulse*.

Table 2.
Injury criteria values and the risk of injury calculated according to the proposed risk functions in [16] from simulations of the state-of-the-art restraint system with the generic 56 km/h FFRB crash pulse and the two car-to-HGV head-on crash pulses.

Crash pulse		**56 km/h FFRB**		**Car-to-HGV long duration crash pulse**		**Car-to-HGV high acceleration crash pulse**	
	Unit	**Value**	**Risk**	**Value**	**Risk**	**Value**	**Risk**
HIC15 (AIS3+)		365	2%	536	6%	2162	62%
BrIC (AIS3+)		0.55	1%	0.58	2%	1.15	74%
Nij (AIS3+)		0.32	1%	0.50	4%	1.42	84%
Chest deflection (3+ fracture 40 years)	mm	40.4	29%	45.7	39%	56.8	61%
Chest deflection (6+ fractures 40 years)	mm	40.4	17%	45.7	24%	56.8	41%
Acetabulum resultant force (AIS2+), 15°	N	3851	71%	4848	94%	20813	100%
Acetabulum resultant force (AIS2+), 0°	N	3851	37%	4848	75%	20813	100%
Femur compression (AIS2+)	N	2683	0%	4887	1%	34697	100%
Upper Tibia axial force (AIS2+)	kN	1.6	1%	2.6	3%	11.0	96%
Lower Tibia axial force (AIS2+)	kN	1.8	5%	2.9	8%	6.9	38%
Tibia bending moment (AIS2+)	Nm	103.9	2%	186.3	11%	1144.6	100%
Revised Tibia index (AIS2+)		0.53	5%	0.92	24%	5.68	100%

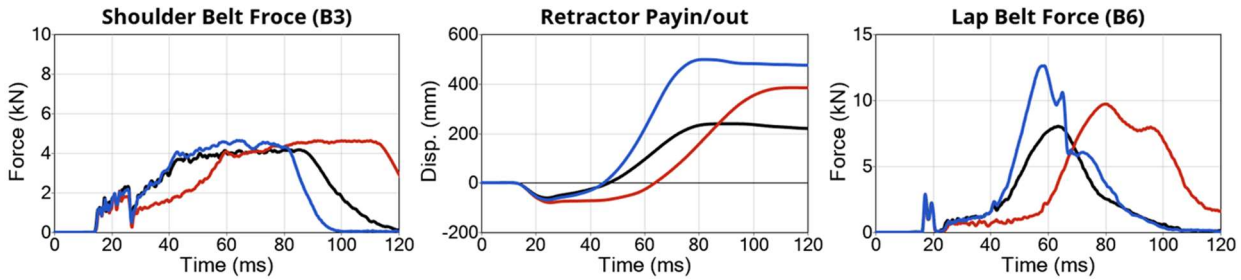

Figure 4. **Left: Upper shoulder belt force. Middle: Retractor belt pay-out. Right: Outer lap belt force. 56 km/h FFRB crash pulse in black, high acceleration crash pulse in blue and long duration crash pulse in red.**

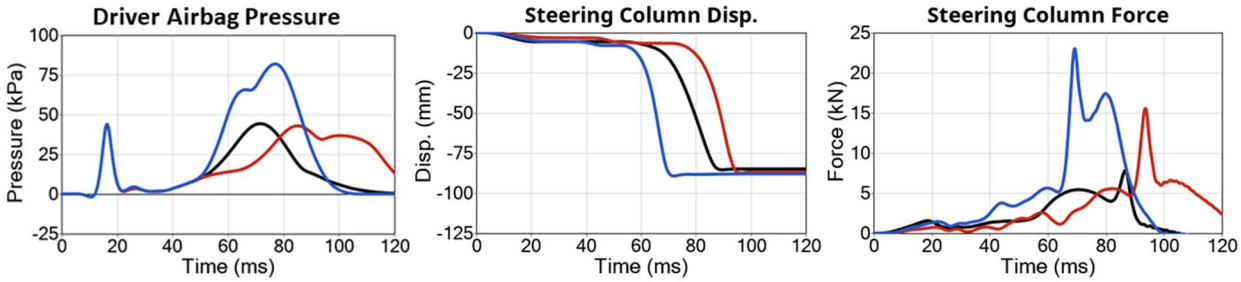

Figure 5. **Left: Driver airbag pressure. Middle: Steering column displacement. Right: Steering column force. 56 km/h FFRB crash pulse in black, high acceleration crash pulse in blue and long duration crash pulse in red.**

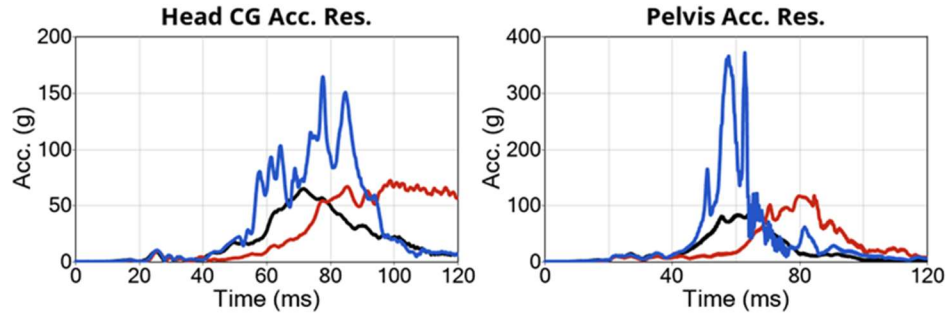

Figure 6. **Left: Head resultant acceleration. Right: Pelvis resultant accelerations. 56 km/h FFRB crash pulse in black, high acceleration crash pulse in blue and long duration crash pulse in red.**

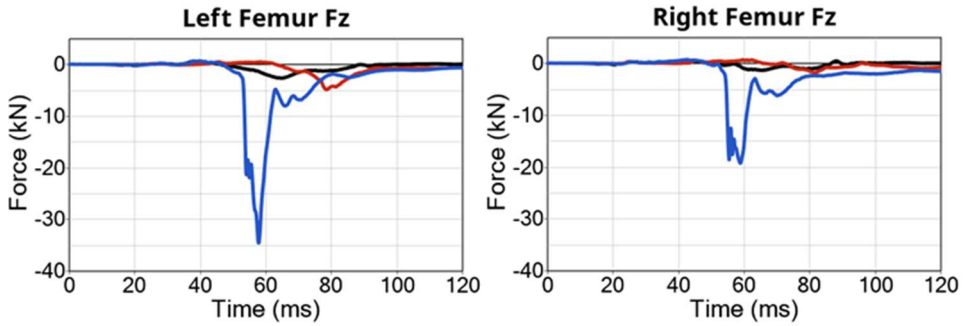

Figure 7. **Left: Left femur compression force. Right: Right femur compression forces. 56 km/h FFRB crash pulse in black, high acceleration crash pulse in blue and long duration crash pulse in red.**

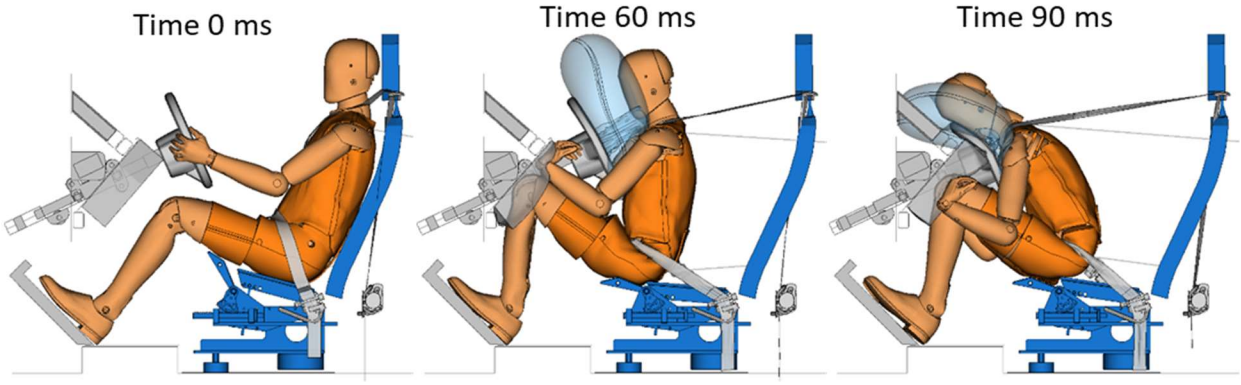

Figure 8. **THOR-50M in the high acceleration crash pulse. Left: Initial position. Middle: Position at maximum pelvis displacement (knee-to-knee bolster strikethrough and pelvis-to-seat pan strikethrough). Right: Position at maximum chest forward displacement (head-to-steering wheel strikethrough).**

Simulation results from car-to-HGV crash pulses with the improved restraint system

With the target to avoid strikethrough of any body part, an improved restraint system was designed in several simulation iterations.

The strikethrough of the pelvis-to-seat pan was addressed by stiffening the seat pan springs until the pelvis strikethrough was avoided.

The strikethrough of the knee-to-knee bolster was addressed by splitting the knee bolster into left and right parts, placing these close to the knees to take load early, and adding load limiters to avoid hard contact to the rigid plate, see

Figure 9. The knee bolster load limiter stroke was 80 mm on the left side and 65 mm on the right side in the *high acceleration crash pulse*.

The strikethrough of the head-to-steering wheel was avoided by increasing the shoulder belt force, from 4 kN to 8 kN, in combination with adding additional 25 mm steering column stroke.

A visualisation of the effect of the improved restraint system to THOR-50M kinematic in the *high acceleration crash pulse* is presented in *Figure 10*. Similar to *Figure 8*, the three figures are at initial position, maximum pelvis displacement, and maximum chest forward displacement. Head-to-steering wheel strikethrough was avoided with a remaining distance of 27 mm and 52 mm for the *high acceleration crash pulse* and the *long duration crash pulses*, respectively. Seatbelt characteristic, driver airbag pressure, steering column characteristic, and strikethrough related measurements (head resultant acceleration, pelvis resultant acceleration and femur forces) of the improved restraint system compared to the state-of-the-art restraint system for the *high acceleration crash pulse* are presented in *Figure 11* to *Figure 14*.

For the improved restraint system, the driver airbag pressure was reduced from above 80 kPa to below 60 kPa (*Figure 12*) and the lap belt force was reduced from approximately 12.5 kN to approximately 8 kN (*Figure 11*).

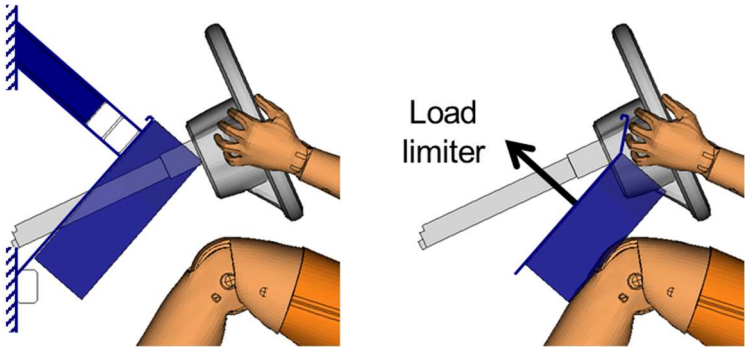

Figure 9. **Left: Knee bolster position in the state-of-the-art restraint system. Right: Knee bolster moved close to the knees in combination with adding load limiters.**

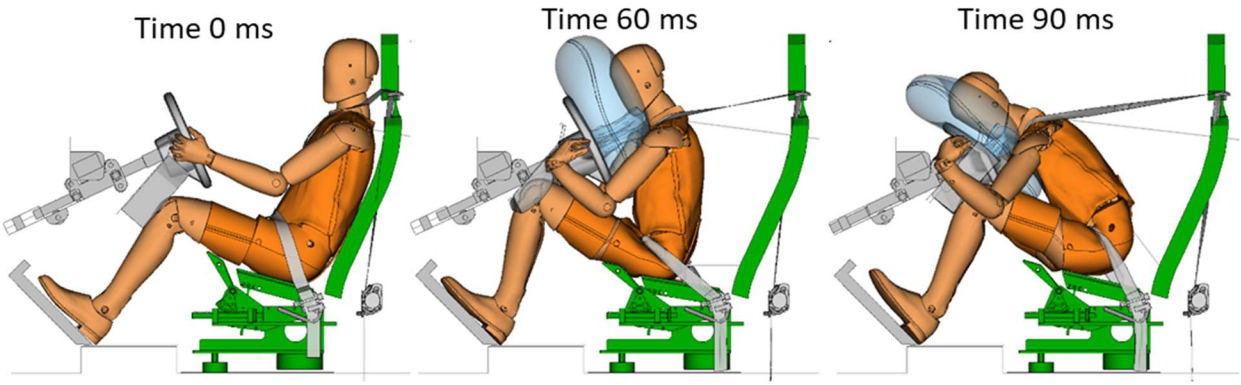

Figure 10. **THOR-50M in the high acceleration crash pulse. Left: Initial position. Middle: Position at maximum pelvis displacement. Right: Position at maximum chest forward displacement with remaining 27 mm to head-to-steering wheel strikethrough.**

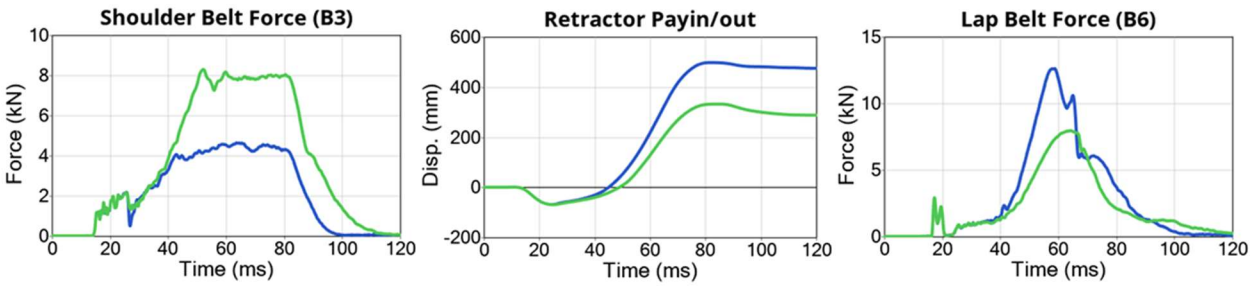

Figure 11. **Left: Upper shoulder belt force. Middle: Retractor belt pay-out. Right: Outer lap belt force. High acceleration crash pulse, state-of-the-art restraint system in blue and improved restraint system in green.**

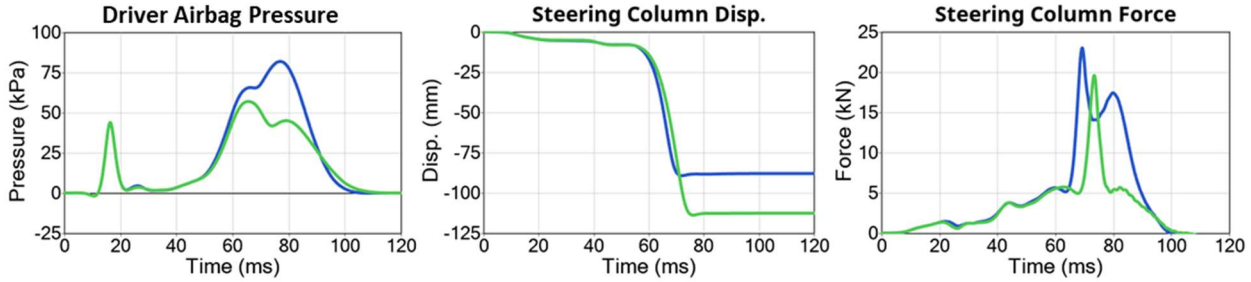

Figure 12. **Left: Driver airbag pressure. Middle: Steering column displacement. Right: Steering column force. High acceleration crash pulse, state-of-the-art restraint system in blue and improved restraint system in green.**

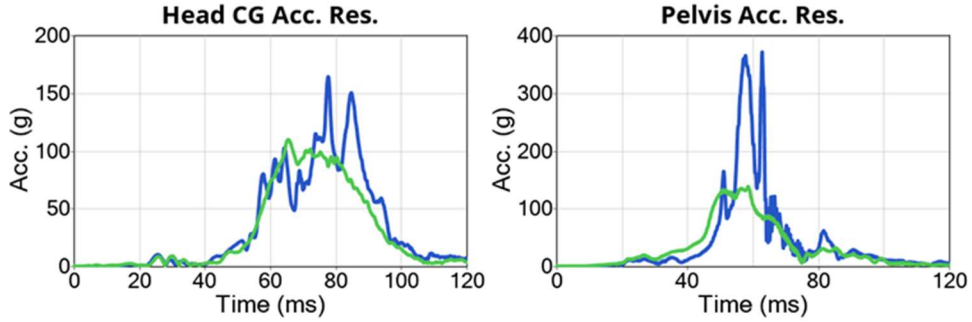

Figure 13. **Left: Head resultant acceleration. Right: Pelvis resultant accelerations. High acceleration crash pulse, state-of-the-art restraint system in blue and improved restraint system in green.**

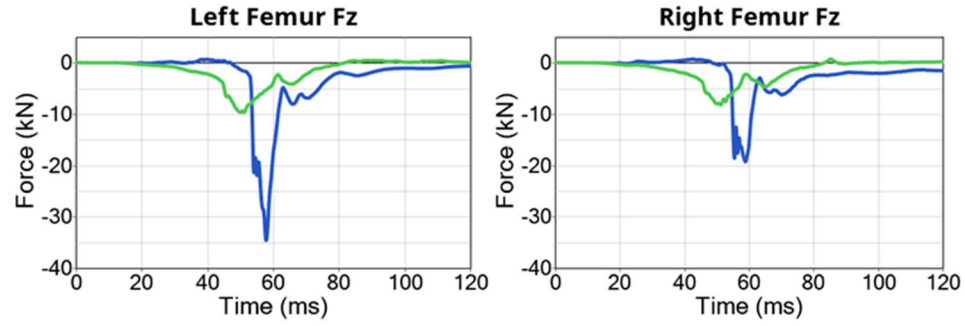

Figure 14. **Left: Left femur compression force. Right: Right femur compression forces. High acceleration crash pulse, state-of-the-art restraint system in blue and improved restraint system in green.**

The improved restraint system met the top initial priorities i.e., avoiding strikethrough for all body regions. The resulting injury criteria values are found in *Table 3*. Overall, the injury criteria values were reduced with the improved system, though some measures remained above the target 40% risk level.

Table 3.
Injury criteria values and the risk of injury calculated according to the proposed risk functions in [16] from simulations of the improved restraint system with the two car-to-HGV head-on crash pulses.

Crash pulse		**Car-to-HGV long duration crash pulse**		**Car-to-HGV high acceleration crash pulse**	
	Unit	**Value**	**Risk**	**Value**	**Risk**
HIC15 (AIS3+)		742	13%	1382	38%
BrIC (AIS3+)		0.63	5%	0.85	33%
Nij (AIS3+)		0.55	5%	0.98	33%
Chest deflection (3+ fracture 40 years)	mm	43.6	35%	56.4	60%
Chest deflection (6+ fractures 40 years)	mm	43.6	21%	56.4	40%
Acetabulum resultant force (AIS2+), 15°	N	3891	73%	5667	99%
Acetabulum resultant force (AIS2+), 0°	N	3891	39%	5667	91%
Femur compression (AIS2+)	N	7124	10%	9742	39%
Upper Tibia axial force (AIS2+)	kN	2.5	2%	3.3	5%
Lower Tibia axial force (AIS2+)	kN	2.7	8%	3.4	10%
Tibia bending moment (AIS2+)	Nm	168.2	8%	234.1	22%
Revised Tibia Index (AIS2+)		0.90	22%	1.23	49%

DISCUSSION

Occupant protection for different crash severities is of high priority. Occupant protection systems should be designed to be adaptative to the crash, i.e., more compliant in low-severity crashes and stiffer in high-severity crashes. Most car crashes occur at a relative low delta velocity [23-24]. While the per-crash risk is relatively low, the high exposure to low-severity crashes leads to most injuries occurring in crashes of relatively low delta velocity [16, 24]. However, this does not contradict that most fatal car crashes occur at relative high crash severity, such as car-to-HGV crashes or car-to-car crashes with high delta velocity. Using FE simulations, we investigated the effect from high severity head-on car-to-HGV crash pulses to the occupant protection with a state-of-the-art restraint system. We identified three critical limitations: head-to-steering wheel strikethrough, knee-to-knee bolster strikethrough and pelvis-to-seat pan strikethrough, all resulting in high risk of injury when evaluated with THOR-50M.

With a more efficient knee bolster that engages the femur early in the crash and is load limited at approximately 10 kN (40% risk of an AIS2+ injury [16]), the kinetic energy of the occupant was effectively managed, and knee-to-knee bolster strikethrough was avoided. This resulted in a high predicted risk of acetabulum fracture, but as stated in [16] the injury risk function for acetabulum as described in [19] might overestimate the risk of acetabulum fractures as such injuries seems to be less frequent than femur fractures in the field [16]. The knee bolster with foam and a load limiting function used in this study can potentially be replicated by a knee airbag by adapting the geometry and pressure to similar shape and stiffness levels.

The seat pan stiffness of the semi-rigid seat was increased to avoid pelvis-to-seat strikethrough. The increased stiffness was implemented because the semi-rigid seat reached its limit in terms of seat pan displacement after approximately 40 mm deflection. The semi-rigid seat was designed to replicate the stiffness of a production seat, but not evaluated in high severity crashes [25]. A stiffer seat than current production seats can potentially be achieved by implementing an inflatable seat pan airbag, also called pelvis restraint cushion [21-22].

The shoulder belt load limiter level was increased from 4 kN to 8 kN. In combination with a somewhat longer steering column stroke, the head-to-steering wheel strikethrough was avoided. In terms of accelerations, forces, and moments the simulation outcomes seem useful, but it seems unlikely that an 8 kN shoulder belt force in combination with the

high acceleration crash pulse would result in less than 20 mm increase of the chest deflection for a human, (40.4 mm chest deflection for the state-of-the-art restraint system in 56 km/h FFRB crash pulse and 56.4 mm chest deflection for the improved restraint system in *high acceleration crash pulse*). Therefore, caution should be taken when interpreting the risk of rib fractures (3+ and 6+) predicted in this study.

By implementing the proposed improvements to the state-of-the-art restraint system, it appears feasible to avoid strikethrough of any body part and thereby increase the occupant protection in high severity collisions. However, despite the improvements explored here, higher injury criteria values than normally seen in NCAP testing were still observed for all body regions. In a parallel study a 40% risk of injury for all body region was proposed for high-severity collision evaluations [16]. Targeting equal risk for all body regions make it possible to rebalance the occupant restraint system compared to current NCAP performance limits, where the risk differs per body region. In addition to the improvements identified here, further reduction of the risk of head injury could potentially be achieved by introducing a dual depth driver airbag [15].

Occupant protection systems are most likely capable of these improvements with existing technologies, although they are currently not designed with the level of adaptivity that this study indicates may be beneficial. Moreover, to activate such adaptive restraint systems correctly would require a sensor system that can identify the crash severity level accurately, either during the first milliseconds of the crash or, ideally, just prior to the crash (e.g., using data streams on the closing velocity combined with sensing classification of the impending collision partner). This could potentially be done by incorporating already present pre-crash sensor data from camera, LIDAR, and RADAR sensors. Today, these are mainly used to avoid crashes and to activate pre-crash functions such as electrical pretensioners of the seat belts [26].

The improved frontal restraint system was shown to be effective in reducing risk of injury in a head-on car-to-HGV crashes with the THOR-50M. However, for the restraint system to work as intended an intact vehicle structure is required. Improvements to the vehicle fleet to increase the compatibility in this type of crashes are fundamental. Incompatibility in terms of geometry and stiffness between cars and HGV often result in that the car underrun the HGV structure [6-11]. The EU project *Improvement of Vehicle Crash Compatibility through the Development of Crash Test Procedures* (VC-COMPAT) [9] identified head-on car-to-HGV crashes as the worst car-to-HGV collision type in terms of the car underrunning the HGV structure. To reduce the risk of the car underrunning the HGV structure, frontal underrun protection devices (FUPD) are obligatory in the EU since August 10, 2003 [27]. However, it is indicated that the structural interaction between cars and HGVs in some cases remain poor, despite the presence of a FUPD [10-11]. To further improve the compatibility in head-on crashes between cars and HGVs, and thereby reduce the risk of injury, it was proposed to fit an energy-absorbing structure to the FUPD [6, 9-10]. Such devices would not only reduce the risk of underrun but also reduce the high acceleration of the car, making head-on car-to-HGV more survivable [6, 9-10]. In crash tests with 75 km/h relative velocity and 75% overlap, it was concluded that equipping the HGV with an energy-absorbing front structure with a force level of 200 kN and 360 mm deformation zone, 30% of the fatal crashes could be avoided, compared to 20% with a 100% rigid FUPD [6]. It appeared that an energy absorbing FUPD may change the severity of a 75 km/h 75% overlap frontal car-to-HGV crash into the severity of a 56 km/h crash [6]. The weights and dimensions directive for HGV, EC 2015/719 was revised to allow additional length of HGVs if the extra length incorporates an energy absorption structure [28] which open up for improved compatibility and energy absorption.

Limitations

This investigation includes several limitations. The frontal sled model was validated to existing sled tests in 40 km/h and 56 km/h FFRB. To expand its usage to a high severity crash pulse reaching 80g is to use the model outside its validation range. In addition to this, all simulations were conducted with a sled-type set-up meaning that no compartment intrusions were included, instead the compartment was rigid. This means, that the risk of strikethroughs might have been underpredicted although the risk of injuries due to strikethroughs was overpredicted. Therefore, focus should be on kinematic criteria rather than on THOR injury criteria values. Strikethrough of a restraint system indicates that the system has reached it limits.

Further work

While first-order gains may be made by adapting restraint systems to crash severity, further refinement will likely require adapting also to occupant characteristics such as stature, mass, and body shape, seat position, and seating posture. Only then will the occupant protection system be truly adaptive. Therefore, we encourage the use of human body models that could be morphed to represent the diversity of the human population and be seated in any seat

position. However, further refinements of human body models are necessary to accurately represent kinematics and to predict injuries in different seating postures as well as in high severity crashes.

CONCLUSIONS

Several limitations in the state-of-the-art restraint system were identified both in terms of occupant kinematic criteria (strikethroughs) and high risk of injury for several body regions. Potential improves was proposed to the knee bolster, seat, seat belt and steering column; all these judged feasible with existing technologies. The improved restraint system met the top initial priorities i.e., avoiding strikethrough for all body regions. Overall, the injury criteria values were reduced with the improved system though some injury criteria values remained above the target 40% risk level.

ACKNOWLEDGEMENTS

The authors want to thank Per-Erik Johansson, Mikael Videby, Sonny Muhoray and Mikael Lindberg all at Autoliv Safety Center in Sweden for executing the sled tests and for their patience when changes were made at the last minute. We would also like to thank Linus Larsson, Nicklas Brunnegård and Stefan Knutsson all at Autoliv Sweden for expertise support in designing the prototype used in the sled tests.

The work was partly carried out as part of the EU project SAFE-UP which has received funding from the European Union's Horizon 2020 research and innovation programme under Grant Agreement 861570.

REFERENCES

[1] European Commission. 2021. Road safety thematic report – Fatigue. European Road Safety Observatory. Brussels, European Commission, Directorate General for Transport. https://road-safety.transport.ec.europa.eu/statistics-and-analysis/statistics-and-analysis-archive/annual-accident-report-archive_en. Accessed 24.10.2022.

[2] European Commission. 2021. Facts and Figures Car occupants. European Road Safety Observatory. Brussels, European Commission, Directorate General for Transport. https://road-safety.transport.ec.europa.eu/system/files/2021-12/F%26F%20Car%20occupants%2020210707.pdf. Accessed 24.10.2022.

[3] Schindler R, Jänsch M, Bálint A, Johannsen H. 2022. Exploring European Heavy Goods Vehicle Crashes Using a Three-Level Analysis of Crash Data. Int J Environ Res Public Health. 2022 Jan 7;19(2):663. doi: 10.3390/ijerph19020663. PMID: 35055484; PMCID: PMC8775486.

[4] European Commission. 2020. European Road Safety Observatory Facts and Figures Buses / coaches / heavy goods vehicles - 2020. Brussels, European Commission, Directorate General for Transport. https://road-safety.transport.ec.europa.eu/system/files/2021-07/facts_figures_buses_and_hgv_final_20210323.pdf. Accessed 24.10.2022.

[5] European Commission, Mobility and Transport. 2021. Road traffic Fatalities in the EU in 2019. https://road-safety.transport.ec.europa.eu/system/files/2021-11/DG%20MOVE%20ROAD%20SAFETY_INFOGRAPHICS_twitter.pdf. Accessed 24.10.2022.

[6] de Coo PJA., Blaauw GJ, Huijbers, JJW. 1997. EEVC working group 14 activities in energy-absorbing front underrun protection. SAE heavy vehicle underride protection TOPTEC, 15-16 April 1997, Palm Springs, CA, USA.

[7] Adalian C, Russo J-L, Cesari D, Desfontaines H. 1998. Improvement of car-to-truck compatibility in head-on collisions. The 16th International Technical Conference on the Enhanced Safety of Vehicles (ESV) Proceedings - Windsor, Ontario, Canada, May 31- June 4, 1998. Paper Number 98-S4-O-12.

[8] Forsman, L. 2002. Compatibility in truck to car frontal impacts. 7th International Symposium on Heavy Vehicle Weights & Dimensions Delft, The Netherlands, Europe, June 2002.

[9] Edwards, M. J. et al. 2007. Improvement of Vehicle Crash Compatibility through the Development of Crash Test Procedures. VC-COMPAT Final Technical Report, Transport Research Laboratory, Crowthorne, UK.

[10] Knight I. 2016. Energy Absorbing Front Underrun Protection for Trucks: Developing a test Procedure. DOI: 10.13140/RG.2.2.32120.75529. Project: Safer Aerodynamic Trucks Apollo Vehicle Safety. https://www.researchgate.net/profile/Iain-Knight/publication/325719308_Energy_Absorbing_Front_Underrun_Protection_for_Trucks_Developing_a_test_Procedure/links/5b1fe45c0f7e9b0e373eccbb/Energy-Absorbing-Front-Underrun-Protection-for-Trucks-Developing-a-test-Procedure.pdf Assessed 07.12.2022.

[11] Thomson R, Fredriksson R, Mroz K, Kruse D, Törnvall F. 2023. Frontal Crash Incompatibility of Heavy Truck in Crash Test with Passenger Car. The 27th International Technical Conference on the Enhanced Safety of Vehicles Conference (ESV), Yokohama, Japan 2023. Paper Number 23-0321.

[12] Kockum S. et al. 2017. Volvo Trucks Safety Report 2017. https://www.volvogroup.com/content/dam/volvo-group/markets/master/about-us/traffic-safety/Safety-report-2017.pdf. Accessed 24.10.2022.

[13] Balint A, Labenski V, Schories L, Leyva PH, Östling M, Schmidt D, Schindler R, et al. 2021. Use Case Definitions and Initial Safety-critical Scenarios. Deliverable 2.6, EU Project SAFE-UP, Grand Agreement No. 861570, 2021. https://static1.squarespace.com/static/5efaed43294db25b18168717/t/627e752a8d7775630d2ea94a/1652454782434/SAFE-UP_D2_6_Use%2Bcase%2Bdefinitions%2Band%2Binitial%2Bsafety-critical%2Bscenarios_.pdf. Accessed 24.10.2022.

[14] Mroz K, Östling M, Lubbe N. 2023. Passenger cars in head-on crashes with heavy goods vehicles: for what severity should future car restraint systems be designed? The 27th International Technical Conference on the Enhanced Safety of Vehicles Conference (ESV), Yokohama, Japan 2023. Paper Number 23-0060.

[15] Pipkorn B, Mellander H, Håland Y. 2005. Car driver protection at frontal impacts up to 80 km/h (50 mph). The 19th International Technical Conference on the Enhanced Safety of Vehicles Conference (ESV), Washington D.C; 2005. Paper Number 05-0102.

[16] Forman J, Östling M, Mroz K, Lubbe N. 2023. Potential Injury Criteria for Collisions with Heavy Goods Vehicles. The 27th International Technical Conference on the Enhanced Safety of Vehicles Conference (ESV), Yokohama, Japan 2023. Paper Number 23-0334.

[17] Mroz K, Östling M, Richardson R, Kerrigan J, Forman J, Gepner B, Lubbe N, Pipkorn B. 2020. Effect of Seat and Seat Belt characteristics on the Lumbar Spine and Pelvis Loading of the SAFER Human Body Model in reclined Postures. Proceedings of the IRCOBI Conference, 2020, Munich, Germany.

[18] Höschele P, Smit S, Tomasch E, Östling M. Mroz K, Klug C. 2021. Generic Crash Pulses Representing Future Accident Scenarios of Highly Automated Vehicles. SAE Int. J. Trans. Safety 10(2):2022, doi:10.4271/09-10-02-0010.

[19] Craig M, Parent D, Lee E, Rudd R, Takhounts E, and Hasija V. 2020. Injury Criteria for the THOR 50th Male ATD. Available at: https://lindseyresearch.com/wp-content/uploads/2021/10/NHTSA-2020-0032-0005-Injury-Criteria-for-the-THOR-50th-Male-ATD.pdf Accessed 24.10.2022.

[20] Östling M, Saito H, Vishwanatha A, Ding C, Pipkorn B, Sunnevång C. 2017. Potential Benefit of a 3+2 Criss Cross Seat Belt System in Frontal and Oblique Crashes. Proceedings of IRCOBI conference, 2017, Antwerp, Belgium.

[21] Baudrit P, Potier P, Petit P, Trosseille X. Vallancien G. 2005. Cadaver and dummy investigation of injury risk with anti-sliding system in case of static deployment. The 19th International Technical Conference on the Enhanced Safety of Vehicles Conference (ESV), Washington DC, 2005. Paper Number 05-0084.

[22] Shaw G, et al. 2018. Pelvic restraint cushion sled test evaluation of pelvic forward motion, Traffic Injury Prevention, 19:3, 250-255, DOI: 10.1080/15389588.2017.1326106.

[23] Hu J, Flannagan C, Bao S, McCoy RW, Siasoco KM, Barbat S. 2015. Integration of Active and Passive Safety Technologies - A Method to Study and Estimate Field Capability. Stapp Car Crash Journal; Ann Arbor Vol. 59, (Nov 2015): 269-296.

[24] Forman J, McMurry T. 2018. Nonlinear models of injury risk and implications in intervention targeting for thoracic injury mitigation, Traffic Injury Prevention, 19:sup2, S103-S108, DOI:10.1080/15389588.2018.1528356.

[25] Uriot J, Potier P, Baudrit P, Trosseille X, Petit P, Richard O, Compigne S, Masuda M, Douard R. 2015. Reference PMHS Sled Tests to Assess Submarining. Stapp Car Crash Journal. Vol 59, 2015.

[26] Fujita K, Fujinami H, Moriizumi K, Enomoto T, Kachu R, Kato H. 2003. Development of pre-crash safety system. The 18th International Technical Conference on the Enhanced Safety of Vehicles (ESV), Nagoya, Japan, May 19-22, 2003.Paper Number 544.

[27] DIRECTIVE 2000/40/EC OF THE EUROPEAN PARLIAMENT AND OF THE COUNCIL. https://eur-lex.europa.eu/LexUriServ/LexUriServ.do?uri=OJ:L:2000:203:0009:0028:EN:PDF Accessed 07.12.2022.

[28] DIRECTIVE (EU) 2015/719 OF THE EUROPEAN PARLIAMENT AND OF THE COUNCIL of 29 April 2015. https://eur-lex.europa.eu/legal-content/EN/TXT/PDF/?uri=CELEX:32015L0719&from=LV Accessed 07.12.2022.

APPENDIX A: VALIDATION OF THE FRONTAL SLED FE MODEL

Frontal sled FE model

The frontal sled FE model used in this study includes generic open versions of Autoliv's detailed global belt component models. The generic open retractor model does not contain details such as different retractor locking behaviour for different retractor types or influence of the initial amount of webbing inside the retractor on the load limiter force. Further, the generic open CLT model lock on predefined time, and the generic open webbing model is a mix of different webbings. Nevertheless, the generic open belt component models have been useful in collaborations when encrypted models have not been accepted.

As described in the Method, the frontal sled model is a generic driver belt-in-seat environment aimed for frontal crashes. This model was initially built up in two versions, belt-in-seat and B-pillar mounted D-loop installations, using Autoliv's detailed global belt component models for the retractor (version 4.1.1), the PLP (version 1.1.3), the crash-locking tongue (version 002), and the webbing with bending beams (version 1.1.6). The frontal sled model was validated to five repeated sled test setups with the THOR-50M. Later, Autoliv's detailed global belt component models were replaced by the generic open versions.

After the open belt component models replaced Autoliv's detailed global belt component models in the frontal sled model, no tuning was done to any part of the model. However, during the validation of the frontal sled model using Autoliv's detailed global belt models, minor tuning of the original models of the knee bolster, the driver airbag, the steering wheel, and the steering column were done to more accurate represent their physical counterparts and to increase run stability. No tuning was done to the Humanetics THOR-50M v1.9 Euro-NCAP version model, to the semi-rigid seat model [1], or to Autoliv's detailed global belt component models since all these already were thoroughly validated. The friction coefficient in the belt guide at the seat-back top was calculated using the belt load cell measurements from the physical sled tests. THOR-50M-to-seat friction coefficients were obtained from earlier studies [1], and THOR-50M friction coefficients for contacts to the driver airbag and the belt webbing were those generally used by Autoliv. All FE sub models were positioned to match the 3D-scans of the physical sled tests. All validation simulations were conducted in LS-Dyna, r9.3.1 R140922, LSTC.

In this appendix, the validation with the belt-in-seat frontal sled model using the open belt component models will be presented.

Conducted physical sled tests

Five repeated test set-ups were performed to validate the frontal sled models with Autoliv's detailed global belt component models, both for the belt-in-seat and for the B-pillar mounted D-loop installations. Here, for the validation of the belt-in-seat frontal sled model using the open belt component models, two of these five set-ups are relevant. The difference between these two is the crash pulse: generic FFRB crash pulses of 40 and 56 km/h, respectively, which has previously been used in several simulation investigations [2-4], *Figure A1*. The tests were performed in a hydraulic-type sled catapult manufactured by Mannesmann Rexroth with maximum acceleration of 50 g.

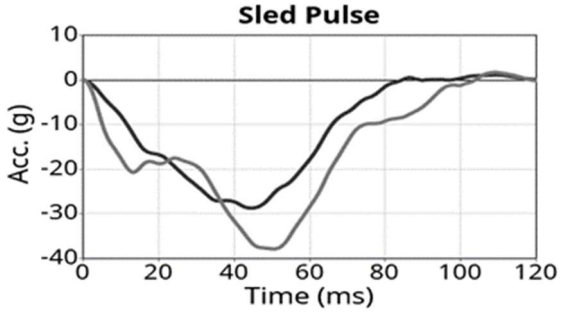

Figure A1. **Crash pulses used in the sled tests. Black curve is the 40 km/h FFRB generic crash pulse and grey curve is the 56 km/h FFRB generic crash pulse.**

The sled set-up represented a state-of-the-art driver restraint system of a mid-sized European car. The set-up includes generic floor geometry and foot support, semi-rigid seat [1], a seat-back to support the occupant, a generic knee bolster

(Ethafoam 220 mounted to a rigid plate), a belt system (belt-in-seat geometry with the belt guide attached to the rigid seat-back, shoulder belt retractor with a 2 kN pretensioner and a 4 kN load limiter, a wire buckle, a crash-locking tongue, and a 2 kN lap belt pretensioner), a generic stroking steering column (force limit of 5.5 kN and a stroke of 85 mm), and a steering wheel with a driver airbag module (coated fabric, vent holes and an dual stage inflator).The THOR-50M was used in all tests and positioned with the H-point 4 mm behind and 29 mm up from the seat reference points

The driver airbag was triggered 10 ms after T0 (crash pulse start). The shoulder belt retractor was triggered 10 ms after T0. The lap belt pretensioner was triggered 15 ms after T0.

Six on-board high-speed cameras recorded the tests at 1000 Hz. The cameras provided images of the left and right side overview, a top and a front view, and left and right side detailed view of the pelvis, its interaction with the seat and lap belt, the lap belt pretensioner, and the buckle and crash locking tongue, *Figure A2*.

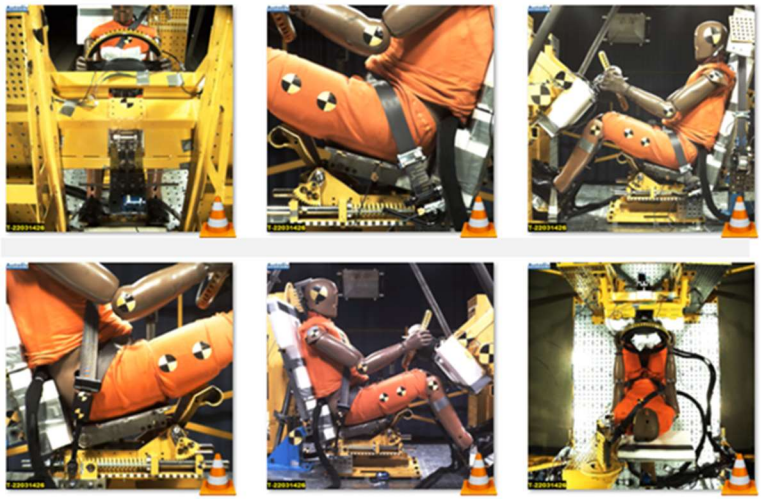

Figure A2. **Overview of the six high-speed camera film views.**

Accelerometer sensors were mounted to the sled to measure the acceleration in the direction of the motion, accelerometer signals were filtered with CFC 60 (*Figure A1*). The shoulder belt retractor included a webbing pay-out sensor to measure webbing pull in and pay-out. Three uniaxial webbing load cells were placed on the seat belt webbing to measure belt forces: just outside the retractor (B1), at the upper shoulder belt between the THOR-50M shoulder and the belt guide (B3), and at the lap belt outboard side between the THOR-50M right hip and the lap belt pretensioner (B6). The webbing load cells signal were filtered with CFC 600. Moreover, the slip in tongues and lap belt pretensioner pay-ins were tracked from videos (*Figure A3 and Figure A4*). Further the airbag pressure was measure with pressure sensors. Pressure signals were filtered with CFC 180. Load cell were mounted between the steering wheel and the steering column to measure the transferred force, these load cell signals were filtered with CFC 180. Four string-potentiometers were used to measure motions. One string-potentiometer was attached to the seat pan, 210 mm from its rotation axis measured in the seat pan plane, to measure seat pan displacement. A second string-potentiometer was attached to the THOR-50M pelvis to measure the forward displacement relative to the sled. A third string-potentiometer was attached to the rear part of the spine at T1 level to measure the chest forward displacement relative to the sled. The fourth string-potentiometer was attached to the steering wheel to measure the steering column stroke. String-potentiometers signals were filtered with CFC 60. All sensors used are listed with manufacturer and model name in *Table A1*. For all sensor signals see *Figure A3* - *Figure A6*.

Table A1
Sensor used in test set-up.

Sensor type	Manufacturer	Model
Webbing load cells	Messring	DK11-35-23
String potentiometers	Space Age	160-1615-C8U9
Webbing pay-out sensor	IES	IES-2098
String potentiometers	Space Age	160-1615-C8U9
Pressure sensors	Kulite	Kulite XTL-142B-190-7BARG
Load cells	Load Indicator	M16-30

The THOR-50M was equipped with the instrumentation specified in the Euro NCAP test protocol [5], including three axis accelerometers in the head, spine (at T1,T4, T12) and pelvis, Infra-Red Telescoping Rods for the Assessment of Chest Compression (IR-TRACCs) for the chest (4) and abdomen (2), six axis load cells (upper neck and femur (left and right), five axis load cells (thoracic spine and tibia (upper, lower, right and left), three axis load cell (forces), left and right acetabulum, two-axis load cells for the anterior superior iliac spines (left and right ASIS), and head, chest and pelvis angular rate sensors. All signals from the THOR-50M were filtered according to SAE J211. The sensors used are listed with manufacturer and model name in *Table A2*. Selected THOR-50M signals are plotted in *Figure A7* to *Figure A20*. One complete 3D scan was performed before one of the tests to facilitate accurate positioning of the THOR-50M and the FE sub models.

Table A2
THOR-50M instrumentation.

Sensor type	Manufacturer	Model
Accelerometers (head, spine and pelvis)	Endevco	7264C-2000
Angular rate head, chest and pelvis	Diversified Technical Systems, Inc	ARS PRO-18K DTS
Upper neck load cell	Humanetics	10380 JI4
Thoracic spine (T12)	Humanetics	10415 JS1I4
IR-TRACCS (Chest and abdomen)	Humanetics	9945
ASIS load cells	Humanetics	10387 JS1I4
Acetabulum right load cells	Humanetics	10670 JS1I4
Acetabulum left load cells	Humanetics	10530 JS1I4
Femur load cells	Humanetics	W50-71010S11
Tibia upper load cells	Denton	3643
Tibia lower load cells	Denton	3644

Frontal sled FE model validation results

Using the generic open belt component models resulted in good matching of the seat belt loads for both crash pulses, but the retractor payout for the 40 km/h crash pulse was a bit too long in simulation model compared to the test measurements, *Figure A3 and Figure A4*.

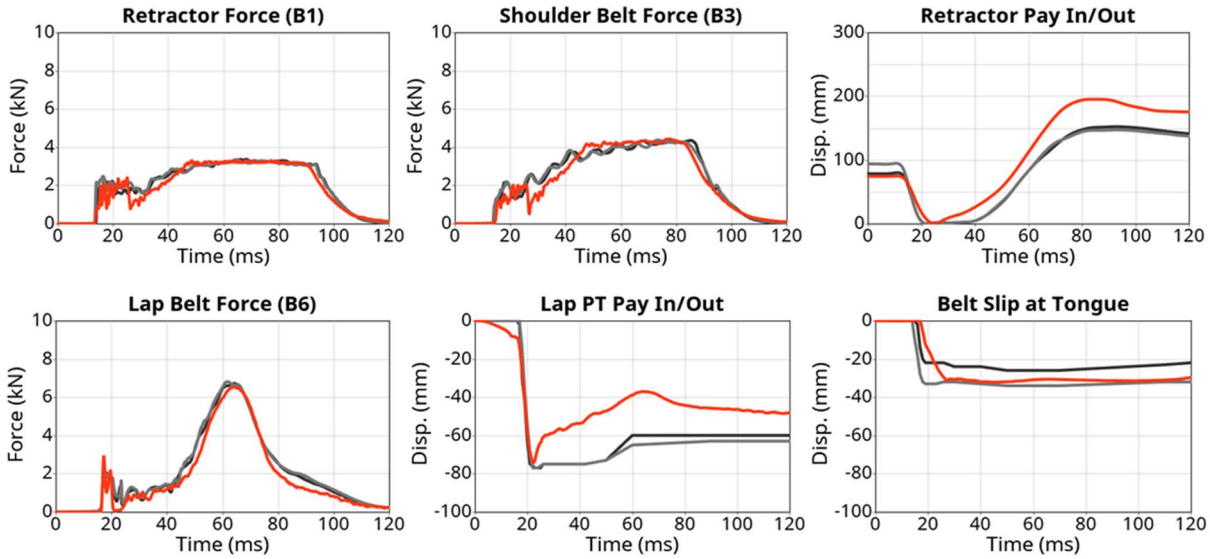

Figure A3. **Belt measurements for 40 km/h crash pulse. Sled curves in grey and simulation curves in red.**

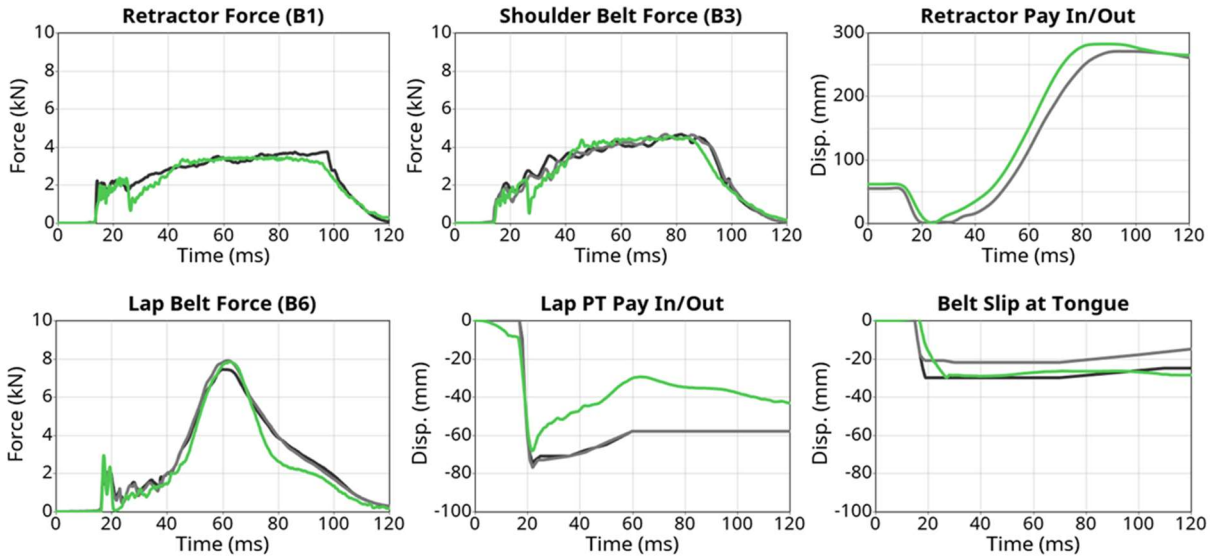

Figure A4. **Belt measurements for 56 km/h crash pulse. Sled curves in grey and simulation curves in green.**

Airbag pressure and steering column force and displacement matched test measurements good for both crash pulses, and so did the seat pan, T1 and pelvis string-potentiometers *Figure A5* and *Figure A6*.

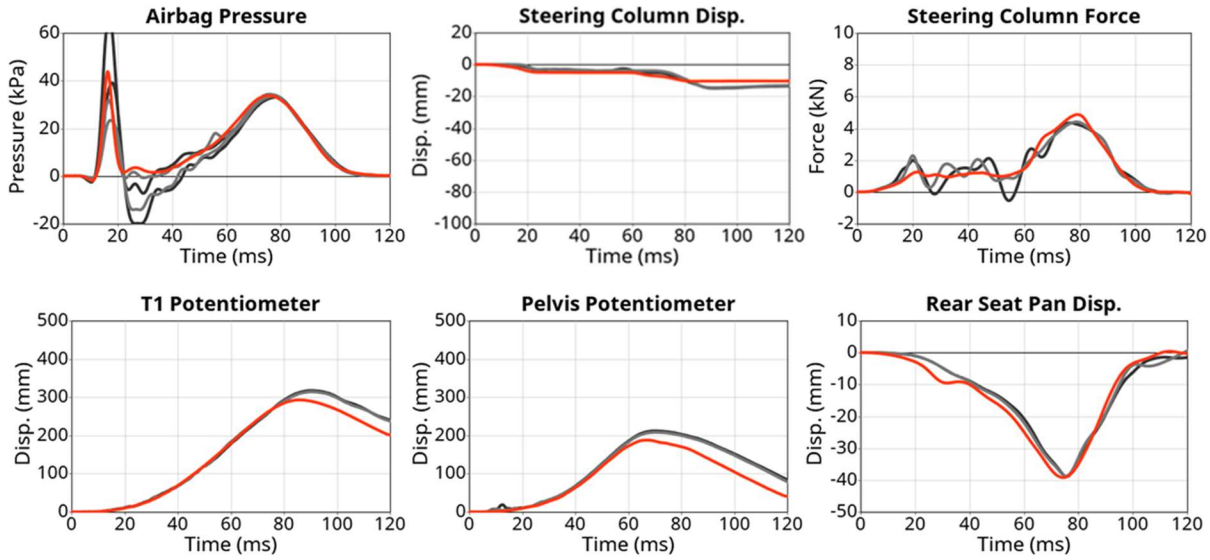

Figure A5. **Measurements for 40 km/h crash pulse. Sled curves in grey and simulation curves in red.**

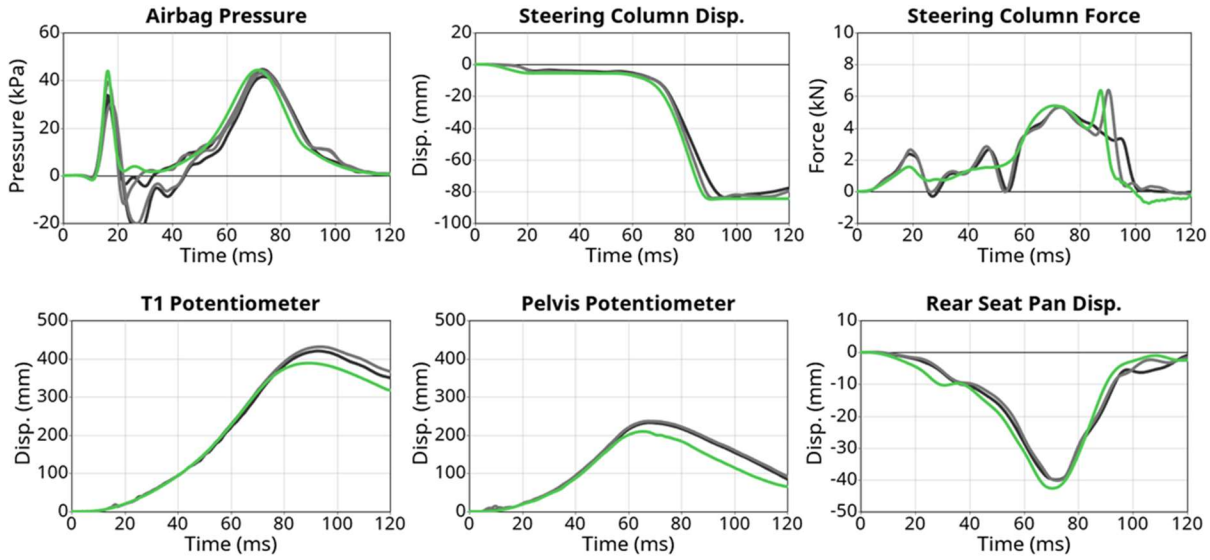

Figure A6. **Measurements for 56 km/h crash pulse. Sled curves in grey and simulation curves in green.**

All simulation acceleration measurements (head, T1, and pelvis) as well as head angular y-velocity, matched test measurements good for both crash pulses. The simulation pelvis angle matched the tests good for both crash pulses, although the rebound phase for the 40 km/h crash pulse was not captured correctly in simulation, *Figure A7* and *Figure A8*. These curves, together with the restraint output and the string-potentiometers, shows that the overall validation of the THOR-50M kinematics is good. Additional validation curves for THOR-50M related signal are shown in *Figure A9* to *Figure A20*.

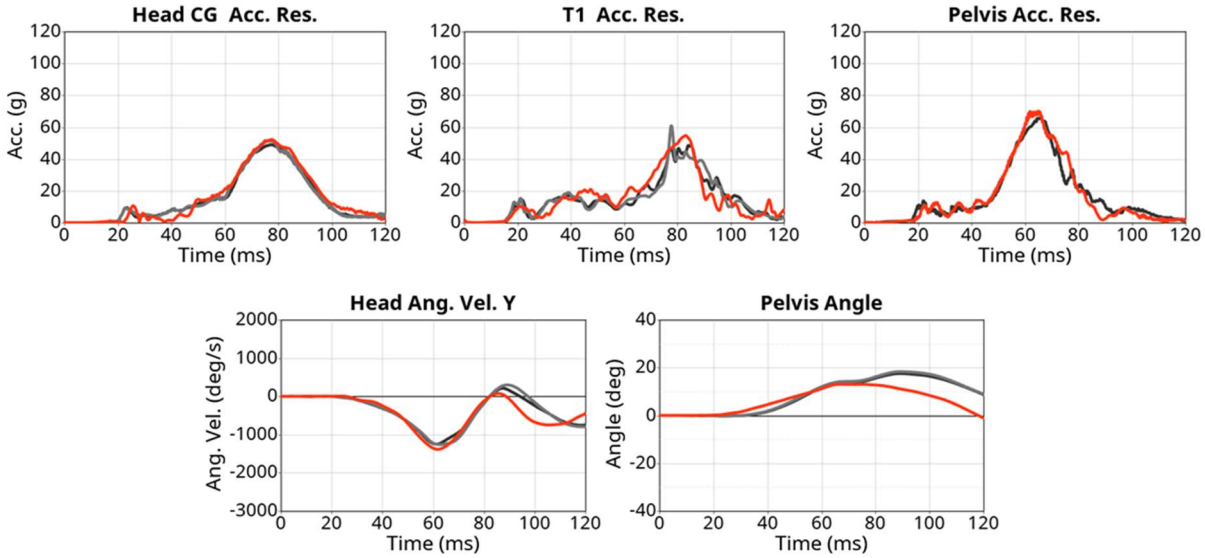

Figure A7. **THOR-50M signals for 40 km/h crash pulse. Sled curves in grey and simulation curves in red.**

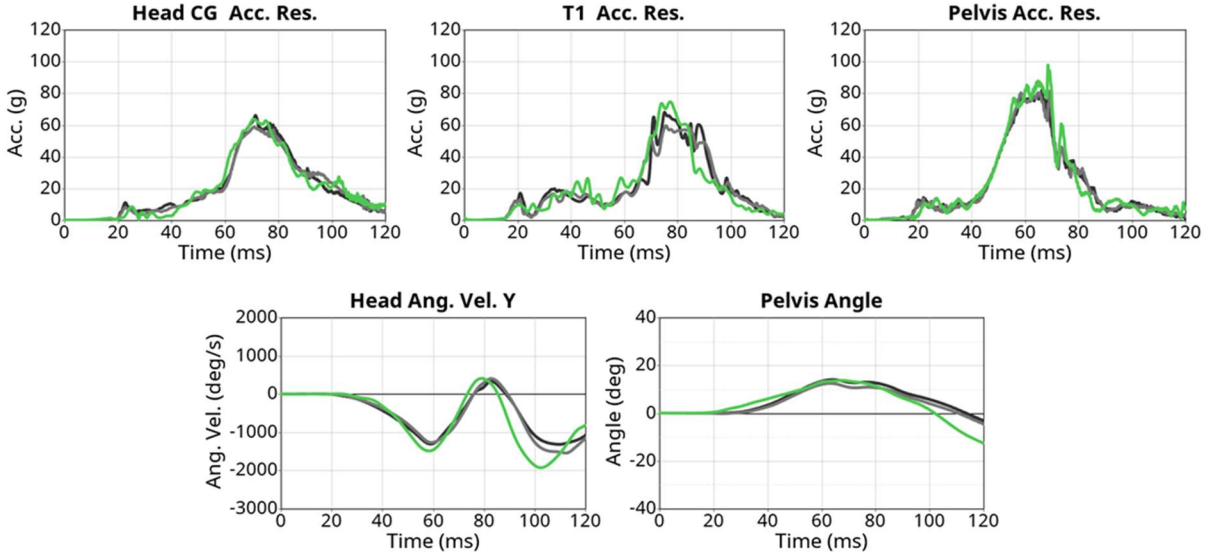

Figure A8. **THOR-50M signals for 56 km/h crash pulse. Sled curves in grey and simulation curves in green.**

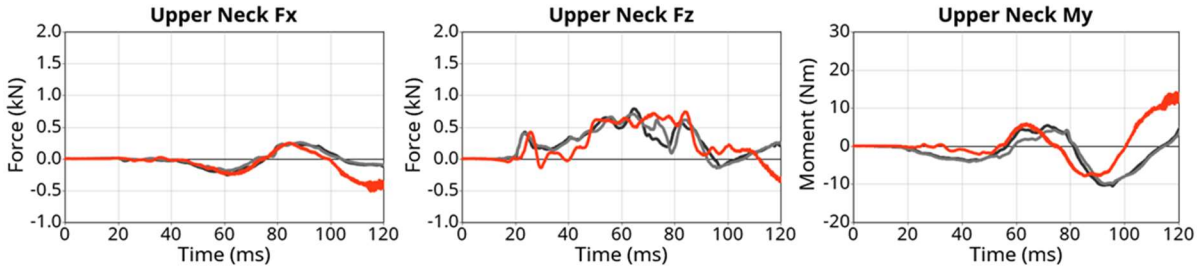

Figure A9. **THOR-50M signals for 40 km/h crash pulse. Sled curves in grey and simulation curves in red.**

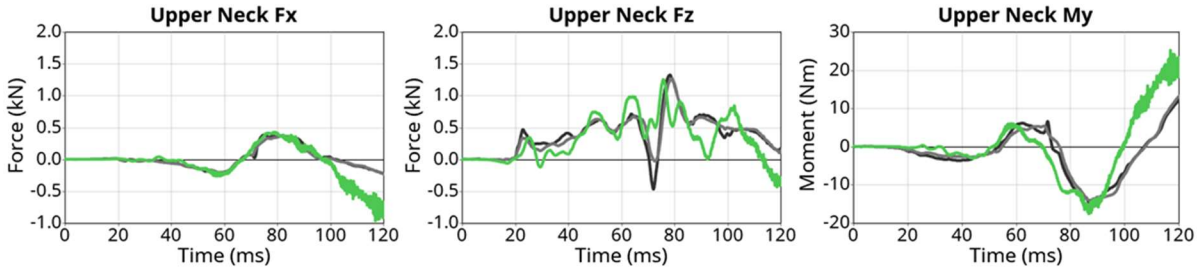

Figure A10. THOR-50M signals for 56 km/h crash pulse. Sled curves in grey and simulation curves in green.

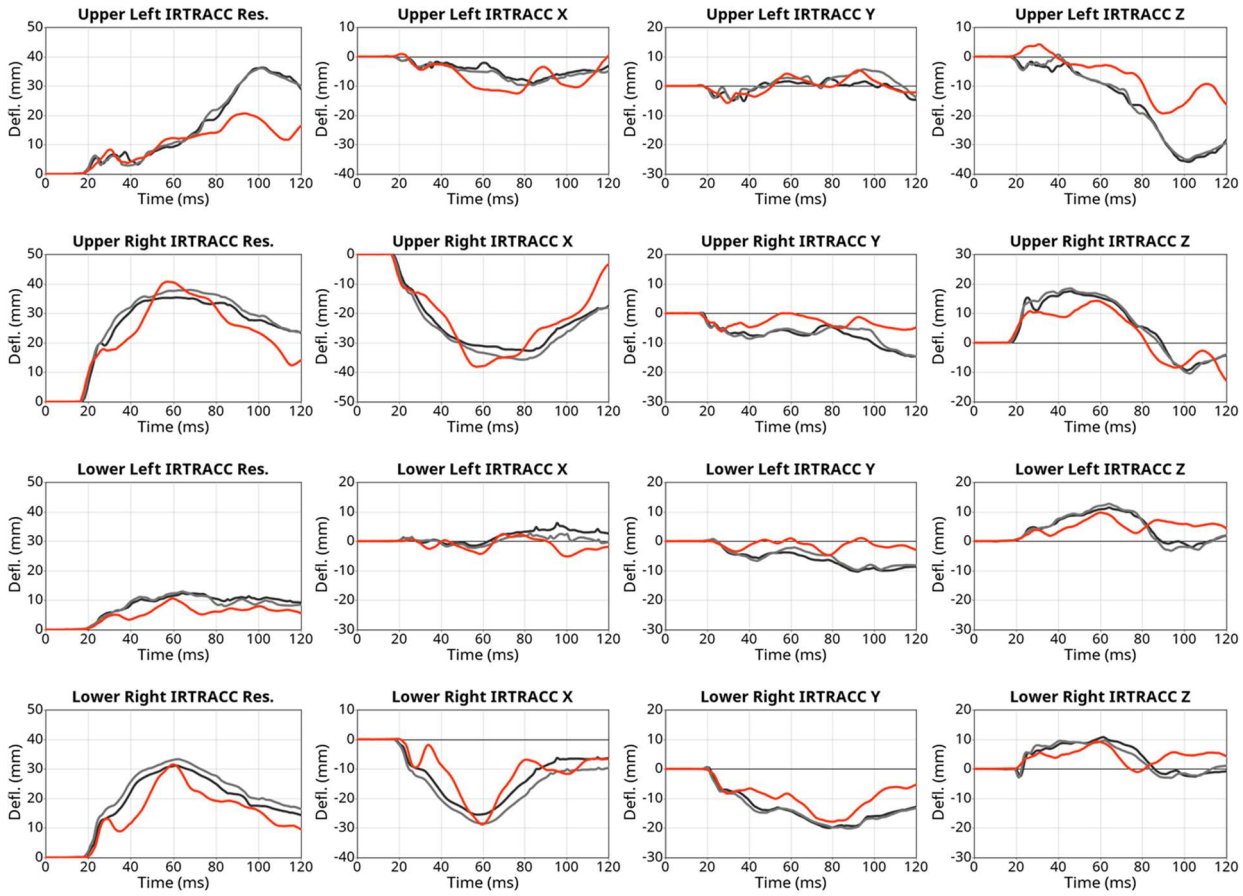

Figure A11. **THOR-50M signals for 40 km/h crash pulse. Sled curves in grey and simulation curves in red.**

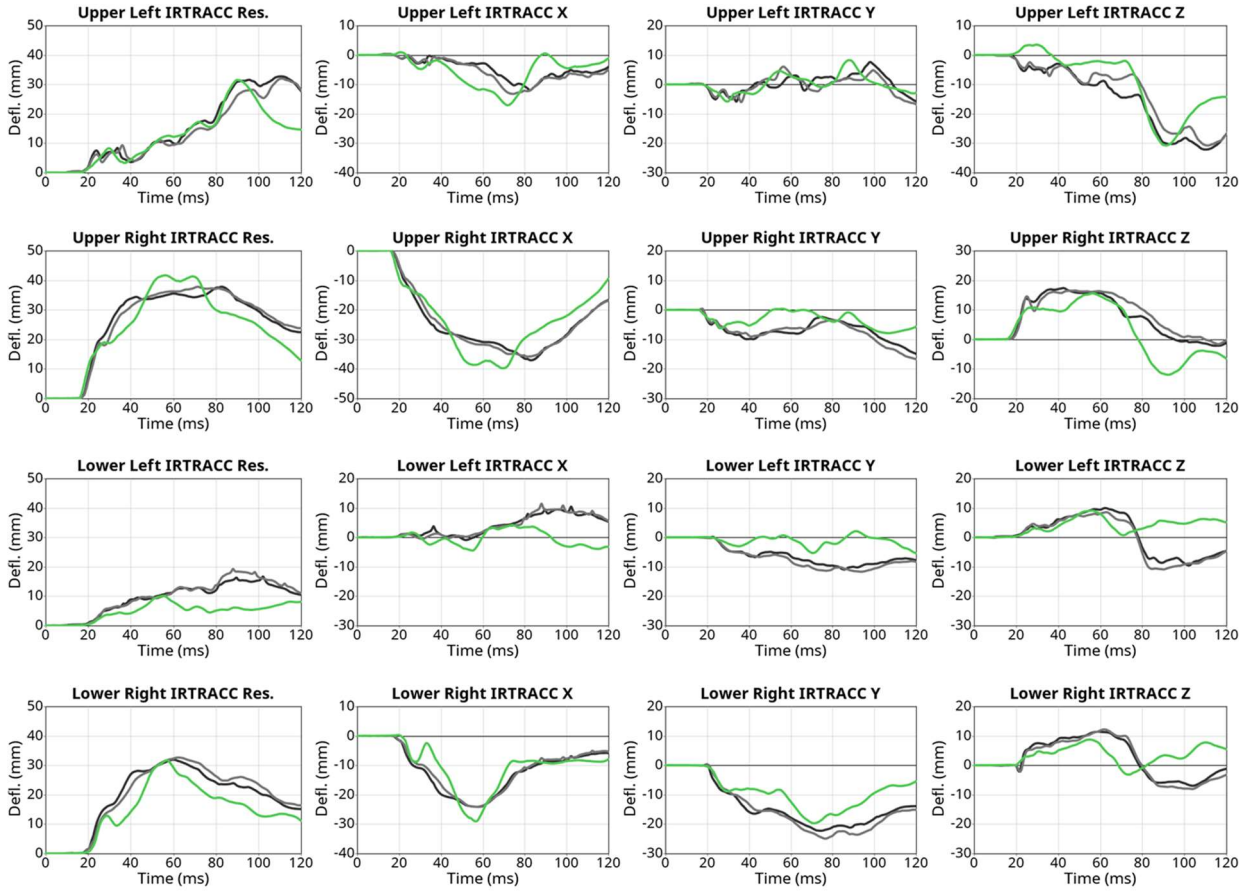

Figure A12. **THOR-50M signals for 56 km/h crash pulse. Sled curves in grey and simulation curves in green.**

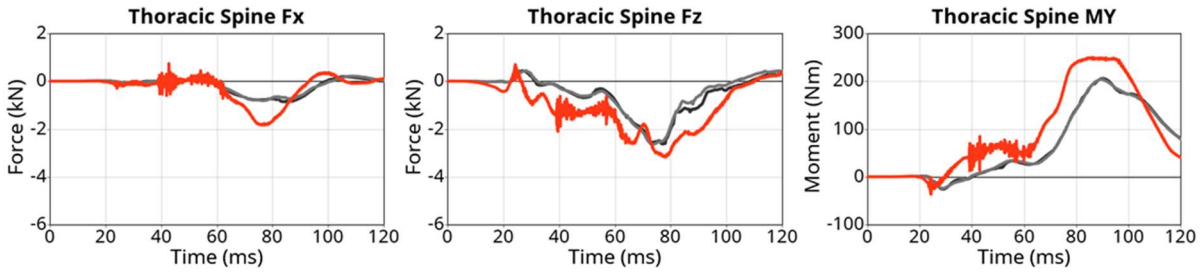

Figure A13. **THOR-50M signals for 40 km/h crash pulse. Sled curves in grey and simulation curves in red.**

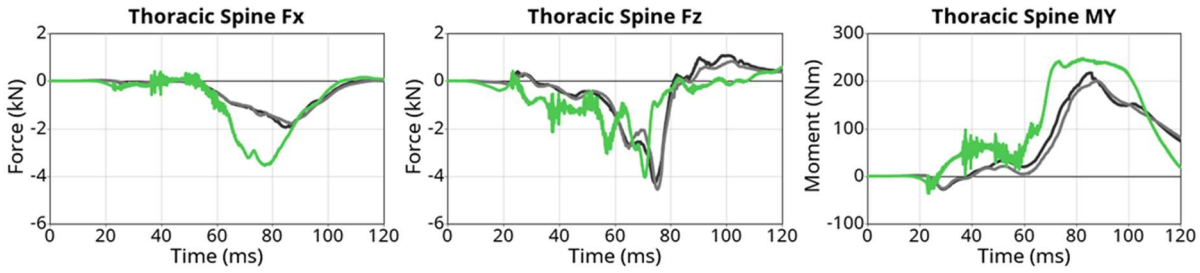

Figure A14. **THOR-50M signals for 56 km/h crash pulse. Sled curves in grey and simulation curves in green.**

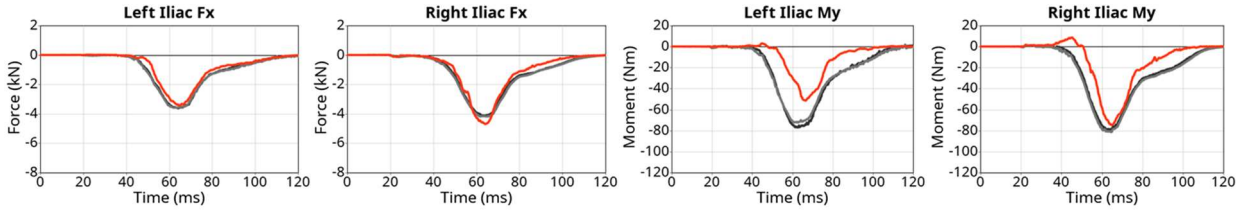

Figure A15. **THOR-50M signals for 40 km/h crash pulse. Sled curves in grey and simulation curves in red.**

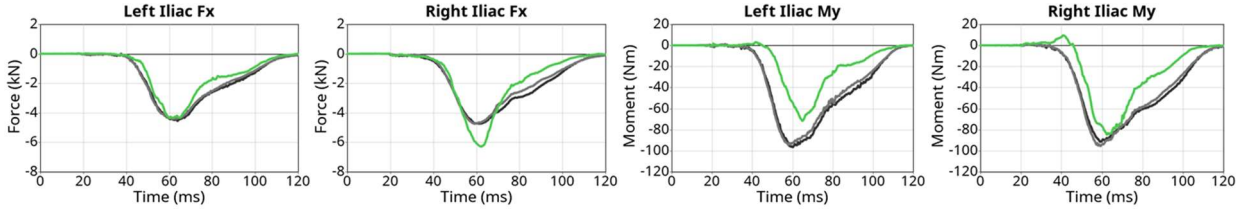

Figure A16. **THOR-50M signals for 56 km/h crash pulse. Sled curves in grey and simulation curves in green.**

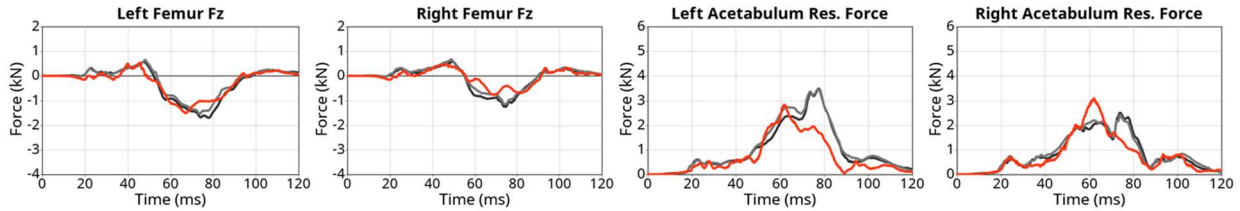

Figure A17. **THOR-50M signals for 40 km/h crash pulse. Sled curves in grey and simulation curves in red.**

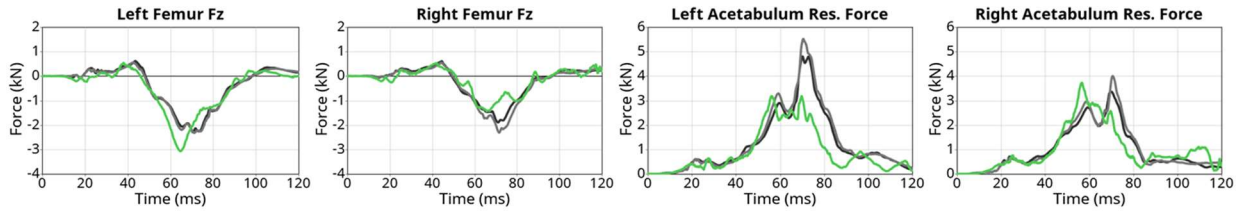

Figure A18. **THOR-50M signals for 56 km/h crash pulse. Sled curves in grey and simulation curves in green.**

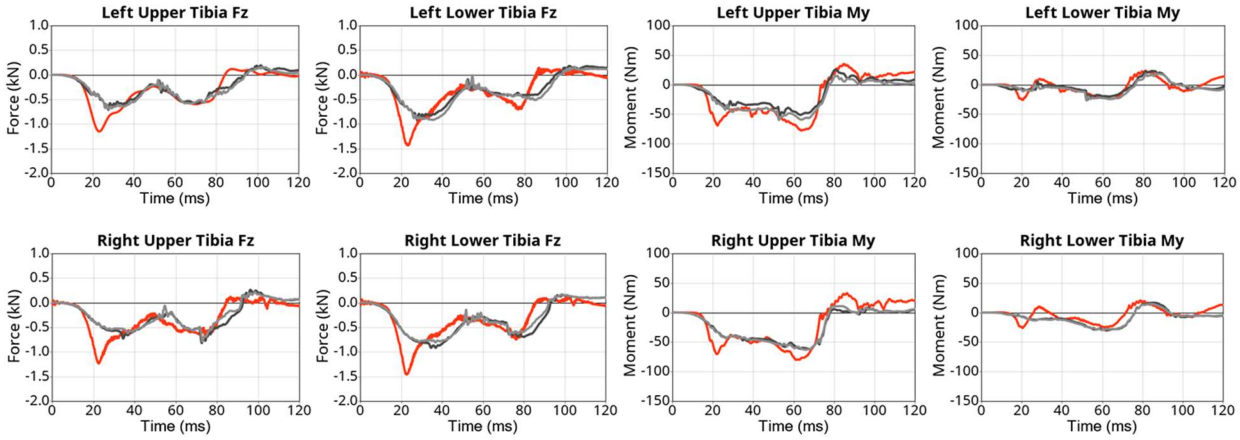

Figure A19. **THOR-50M signals for 40 km/h crash pulse. Sled curves in grey and simulation curves in red.**

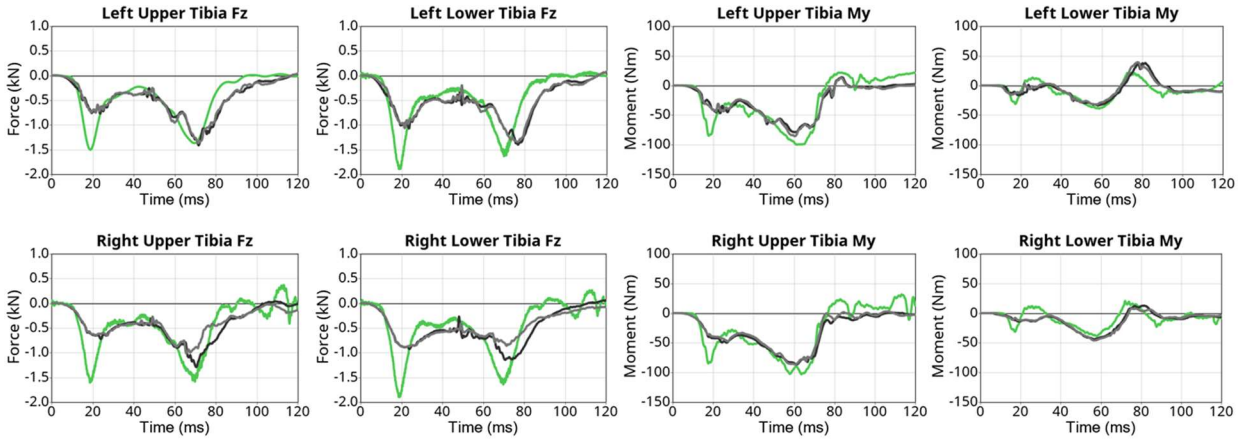

Figure A20. **THOR-50M signals for 56 km/h crash pulse. Sled curves in grey and simulation curves in green.**

REFERENCES

[1] Mroz K, Östling M, Richardson R, Kerrigan J, Forman J, Gepner B, Lubbe N, Pipkorn B. 2020. Effect of Seat and Seat Belt characteristics on the Lumbar Spine and Pelvis Loading of the SAFER Human Body Model in reclined Postures. Proceedings of the IRCOBI Conference, 2020, Munich, Germany.

[2] Schiessler M., et al. 2021. Validation and Demonstration of Advanced Passenger Protection Principles. Deliverable D2.5; OSCCAR Project; Grant Agreement No. 768947; 2021. https://www.osccarproject.eu/media/deliverables/ Accesses 01.12.2022.

[3] Höschele P, Smit S, Tomasch E, Östling M. Mroz K, Klug C. 2021. Generic Crash Pulses Representing Future Accident Scenarios of Highly Automated Vehicles. SAE Int. J. Trans. Safety 10(2):2022, doi:10.4271/09-10-02-0010.

[4] Mroz K, Östling M, Klug C, Höschele P, Lubbe N. 2021. Supplementing Future Occupant Safety Assessments with Severe Intersection Crashes Selected Using the SAFER Human Body Model. SAE Int. J. Trans. Safety 10(2):2022, doi:10.4271/09-10-02-0011.

[5] EUROPEAN NEW CAR ASSESSMENT PROGRAMME (Euro NCAP) ASSESSMENT PROTOCOL – ADULT OCCUPANT PROTECTION Implementation 2023 Version 9.2.1 14th November 2022. https://cdn.euroncap.com/media/75471/euro-ncap-assessment-protocol-aop-v921.pdf. Accessed 05.12.2022.